Aluminizing by pack cementation to protect CoSb3 from oxidation

Richard Drevet, Carine Petitjean, Nicolas David, Lionel Aranda, Delphine Veys-Renaux, Patrice Berthod

Version of Record: https://www.sciencedirect.com/science/article/pii/S0254058419312325
Manuscript_b738222b943e5c895edca89ab11ba954

Aluminizing by pack cementation to protect $CoSb_3$ from oxidation

Richard DREVET*, Carine PETITJEAN, Nicolas DAVID, Lionel ARANDA, Delphine VEYS-RENAUX, Patrice BERTHOD

Institut Jean Lamour, CNRS - Université de Lorraine, UMR 7198, Campus Artem, allée André Guinier, BP 50840, 54011 Nancy cedex, France.

* corresponding author.

Tel.: +33.372.74.27.29.

e-mail address: richarddrevet@yahoo.fr

ABSTRACT

The $CoSb_3$ skutterudite compounds are thermoelectric materials used to produce electricity from heat. Unfortunately, these materials quickly oxidize in air at elevated temperature. To solve this problem, this work explores the possibility to produce a protective aluminide surface layer to limit the interactions with oxygen. To synthesize the layer, this research work experiments the pack cementation process. A good understanding of the process requires the knowledge of the thermodynamic phase equilibria of the involved elements. However, this ternary system has never been considered in literature. Therefore, the first part of the research concerns the study of the isothermal section at 600 °C of the Al-Co-Sb ternary system to improve the knowledge of the phases that can be formed during the pack cementation process. Next, the aluminide surface layer is synthesized, then characterized by coupling scanning electron microscopy (SEM), energy dispersive X-ray spectroscopy (EDS) and X-ray diffraction (XRD) analysis. The results reveal that the obtained coating is made of two crystalline phases, AlSb is the major one and Al_9Co_2 is the minor one. At last, the oxidation

experiments point out the protective properties of the surface layer against oxygen penetration, keeping the substrate safe for 1000 h under a flow of synthetic air at 527 °C. Consequently, the aluminized $CoSb_3$ is a promising thermoelectric material usable in oxidative environments.

Keywords: aluminizing, cobalt-antimony, ternary system, thermoelectric material, oxidation

1. Introduction

The skutterudite compounds made of cobalt (Co) and antimony (Sb) such as $CoSb_3$ are powerful thermoelectric materials thanks to a high figure of merit (ZT > 1) [**1-3**]. $CoSb_3$ is commonly used to produce thermoelectric generators able to convert heat into electrical energy [**4-6**]. These generators are mainly employed in the aerospace industry, more particularly to produce electricity for the space vehicles launched far away from Earth. Currently, many research efforts aim at developing their use on Earth under oxidative environment [**7**]. Actually, their sensitivity to thermal degradation under oxidation mechanisms is a significant problem with regards to their high operating temperatures (several hundreds of Celsius degrees). Numerous studies have highlighted a quick deterioration of the $CoSb_3$ material under a flow of oxygen at high temperature. For example, Godlewska *et al.* have observed the formation of Sb_2O_4, $CoSb_2O_4$ and $CoSb_2O_6$ at the surface of $CoSb_3$ during oxidation in air at 500 °C for eighty hours [**8**]. Hara *et al.* have established that two surface layers are formed during this oxidation treatment [**9**]. They have demonstrated that the outer layer is composed of a mixture of antimony oxides (β-Sb_2O_4 and Sb_2O_3), and the inner layer is made of a mixture of four oxides ($CoSb_2O_6$, $CoSb_2O_4$, Sb_2O_3 and β-Sb_2O_4). Moreover, they have described the parabolic behavior of the oxides layer growth as a function of time, proposing a three-step mechanism of oxidation: (i) antimony diffusion towards the surface, (ii) oxygen penetration into the region of antimony segregation, and then (iii) oxides formation. These reactions promote the degradation of the thermoelectric properties of the material and the decrease of the device sustainability [**10**]. Consequently, a protective surface coating is necessary to prevent the oxidation reactions and the loss of the thermoelectric properties [**11**]. Several coating processes have been studied in literature such as magnetron-sputtering to produce Cr-Si or Ti coatings [**8,11**] and the sol-gel process to synthesize composite glass layers [**12**]. The perspective to use a metallic coating with a great

affinity with oxygen appears to be the most relevant way to solve the oxidation problem. An appropriate solution could be to develop an aluminide layer on $CoSb_3$ by pack cementation, a variant of chemical vapor deposition (CVD). This outlook is very attractive since pack cementation produces adherent coatings unaffected by the high temperatures [**13**]. Moreover, due to its great affinity with oxygen, the aluminide layer is expected to act as a barrier to oxygen, forming alumina (Al_2O_3, a stoichiometric oxide) and preserving the substrate from any deterioration. The pack cementation process consists in the diffusion under vacuum at 600 °C of aluminum atoms inside the alloy [**14-15**]. In literature, the three binary thermodynamic systems constituted by Al, Co or Sb are well known and they have been already studied [**16-22**]. Unfortunately, the Al-Co-Sb ternary system has never been explored. That is the reason why the present research work aims at studying the isothermal section of this ternary system at the temperature used for the coating process, i.e., 600 °C. In a first part, the predicted section of the ternary system is proposed after the presentation of the corresponding binary borders. The experimental study of the different regions is conducted to assess some prospective solubility or ternary compounds which are not predictable by the initial calculation. Then, the aluminide layer synthesized on the $CoSb_3$ substrate is characterized to highlight the phases formed during the process. At last, the oxidation behavior of the coated $CoSb_3$ is assessed under a flow of synthetic air at 527 °C for 1000 hours.

2. Literature review of the binary borders

2.1. Co-Sb equilibrium phase diagram

The commonly accepted phase diagram of the Co-Sb system is shown in **Fig.1** [**21**]. The liquidus line overall decreases between the melting temperature of Co and that of Sb as a function of the Sb content increases. The maximum solubility of Sb is very low (up to 5 wt.%

Sb at 1118 °C) and particularly insignificant below 600 °C in the austenitic cobalt solid solution $(Co)_{ht}$. It is negligible in the hexagonal $(Co)_{rt}$ one whatever the temperature. Similarly the solubility of Co in the antimony solid solution (Sb) is very low (about 0.5 wt.% Co at 631 °C). This diagram also evidences an intermediate solid solution CoSb whose composition varies around 65 wt.% Sb (62 wt.% Sb at 1118 °C to 70 wt.% Sb at 936 °C). It is noticeable that this phase exhibits a congruent melting at 1220 °C. In addition, there are two defined Sb-rich compounds: $CoSb_2$ and $CoSb_3$. It may be noticed that the first one has a polymorphic transition from $(CoSb_2)_{rt}$ to $(CoSb_2)_{ht}$ at 377 °C. Both defined compounds are characterized by a peritectic solidification (936 °C for $CoSb_2$ and 874 °C for $CoSb_3$). **Table 1** and **Table 2** respectively propose the crystallographic description of all the phases and the invariant reactions of the Co-Sb binary system [**23**].

2.2. Al-Co equilibrium phase diagram

The well-accepted phase diagram of the Al-Co system is shown in **Fig.2** [**16**]. It is split in two parts by an intermediate solid solution (AlCo) characterized by a congruent melting (1640 °C). The corresponding domain of this phase extends towards the Co side up to 87 wt.%. The Co-rich side presents a eutectic equilibrium (1401 °C) and a eutectoid equilibrium (300 °C) linked to the two allotropes of cobalt. In the Al-rich part of the diagram, the liquidus line decreases between the congruent melting temperature of (AlCo) and the melting temperature of pure aluminum. Between (AlCo) and (Al), four stoichiometric compounds are defined (Co_2Al_9, Co_4Al_{13}, $CoAl_3$ and Co_2Al_5). All of them have a peritectic solidification (respectively 974 °C, 1104 °C, 1140 °C and 1168 °C). Co_2Al_9 and (Al) define a eutectic equilibrium with the liquid at a temperature close to that of the melting of pure Al (659 °C). It may be noticed that there is no significant solubility of Co in (Al) and also of Al in $(Co)_{rt.}$. In contrast, $(Co)_{ht.}$ presents an important solubility for aluminum (up to 8.6 wt.%). **Table 1** and **Table 2**

respectively provide the crystallographic description of all the phases and the phase equilibria in the Al-Co system [**23**].

2.3. Al-Sb equilibrium phase diagram

The phase diagram of the Al-Sb system displayed in **Fig.3** exhibits a defined compound AlSb characterized by a congruent melting (1055 °C) that cuts the phase diagram in two sides [**19**]: AlSb is in eutectic equilibrium with both pure elements Al (658 °C) and Sb (620 °C). It may be noticed that there is no solubility of antimony in (Al) and no solubility of aluminum in (Sb). **Table 1** and **Table 2** respectively present the crystallographic description of the phases and the phase equilibria in the binary system Al-Sb [**23**].

3. Materials and Methods

3.1. Calculation of the predictive Al-Co-Sb ternary isothermal section

To our knowledge, the Al-Co-Sb ternary system has never been studied in literature. In a first time, the binary Calphad modeling of Co-Sb due to Zhang *et al.* [**21**], of Al-Co due to Stein *et al.* [**16**] and Al-Sb due to Balakumar and Medraj [**19**] were selected. The phase diagrams of these three binary systems are plotted in weight percent in **Fig.1**, **Fig.2** and **Fig.3**, respectively. In the Calphad method, the Gibbs energies of phases are described using mathematical models in which some coefficients should be adjusted. They are obtained on the basis of selected available experimental data with regards to the phase equilibria and the thermodynamic properties of the considered system. These three binary databases are compatible to one another. Consequently, a thermodynamic database including them was created. A predictive calculation of the equilibria between all the phases was done at 600 °C. The corresponding phase diagram is presented in weight percent in **Fig.4**. One should note that the database can only predict possible equilibria between the phases issued from the

binary borders, and it does not indicate possible ternary solubilities or the existence of ternary compounds. The obtained diagram shows a biphasic equilibrium between AlCo and AlSb splitting the isothermal section in two parts. The Al-rich side displays equilibria between Al_xCo_y and AlSb. The CoSb border displays equilibria between Co_xSb_y and AlCo. The isothermal cut being only predictive, it requires experimental investigations.

3.2. Synthesis of the materials for the thermodynamic study

In order to explore experimentally some areas of the isothermal section, eight samples made of a mixture of various amounts of aluminum powder (99.5 %, 7-15 µm, Alfa Aesar®), cobalt powder (99.5 %, 15 µm, Touzart et Matignon®) and antimony powder (99.9 %, 20 µm, Alfa Aesar®) were compacted in air at 300 bar with a hydraulic press to obtain pellets. Afterwards each pellet was put inside an alumina crucible, itself inside a silica ampoule sealed under a dynamic secondary vacuum (10^{-6} mbar) to avoid any oxidation of the samples during the thermal treatment. Then, the whole system was treated at 600 °C for 10 days inside a muffle furnace (Nabertherm), then followed by water quenching.

3.3. Synthesis of the aluminide coating

The chemical process used to coat the $CoSb_3$ substrate is pack cementation. The $CoSb_3$ pellet is a lab-made sample obtained from $CoSb_3$ powder (5 µm in diameter, 99.99 %, synthesized by powder metallurgy), densified by spark plasma sintering (SPS) [**24**]. First, the surface of the $CoSb_3$ pellet is polished with SiC papers and ultrasonically cleaned in ethanol. Then, the pellet is positioned under a dynamic secondary vacuum (10^{-6} mbar) inside a sealed silica ampoule that contains a mixture of powders, i.e. Al (the element to be deposited), Al_2O_3 (inert filler powder) and a small amount of $CrCl_3$ (the halide salt activator). Next, the ampoule is exposed to 600 °C in a muffle furnace (Nabertherm) for 30 minutes. At this temperature, the

aluminum atoms diffuse inside the $CoSb_3$ substrate and react with the cobalt and antimony atoms to produce a metallic coating at the surface of the material [**14**]. At last, the silica ampoule is air quenched at room temperature.

3.4. Characterization of the obtained phases

The crystalline phases of the synthesized samples are assessed by X-ray diffraction (XRD) with a Philips X'pert pro diffractometer using a monochromatic $Cu_{K\alpha}$ radiation (λ=0.15406 nm). The patterns were collected from $2\theta = 20°$ to 60° with a step of 0.01671°. The phases are identified using the diffraction files provided by the International Centre for Diffraction Data (ICDD). Moreover, the cross-sections of the samples are observed from backscattered electron (BSE) images with a scanning electron microscope (SEM, JEOL JSM 6010LA) equipped with an energy dispersive X-ray spectrometer (EDS). At last, X-ray elemental mapping of the cross-section of the coated substrate is carried out at 15 kV.

3.5. Oxidation of the coated skutterudite

The oxidation of the coated $CoSb_3$ skutterudite was carried out at 527 °C for 1000 h in a tubular furnace (Carbolite). A flow of synthetic air, i.e. a mix of dioxygen (20% O_2) and dinitrogen (80% N_2), was injected continuously inside the furnace at 4 $L.h^{-1}$.

4. Results and Discussion

4.1. Experimental study of the isothermal section

The eight studied compositions are positioned on the isothermal section displayed in **Fig.4**. All the samples are characterized after 10 days of thermal treatment at 600 °C under secondary vacuum. The corresponding XRD patterns are reported in **Fig.5**. Various phases' mixtures are identified depending on the initial composition, i.e. the amount of Co, Sb or Al.

It is noteworthy that all the peaks of the eight XRD patterns are attributed to phases of Co, Sb or Al without any oxide phase of these elements. This observation indicates that the secondary vacuum used during the experiments is appropriate to avoid any oxidation of the samples during the thermal treatment. The whole results are collected in **Table 3**. Among the observed phases, AlSb is the only one constituted by aluminum and antimony whereas many other phases contain cobalt: AlCo, Al_5Co_2, Al_9Co_2, $Al_{13}Co_4$, or CoSb, $CoSb_2$, $CoSb_3$. Particularly, all the diffraction peaks are indexed, meaning that there is no ternary phase put in evidence from XRD. Next, the inside of the eight samples is observed using SEM in BSE mode. Two of the obtained micrographs are displayed in **Fig.6** and **Fig.7**. They highlight areas with various contrasts that correspond to the different phases formed during the thermal treatment. The elemental quantifications extracted from the EDS results match with the chemical composition of the phases identified by XRD. They are gathered in **Table 3**. For example, three phases are observable for the C1 sample (**Fig.6**). The EDS analysis locally provides the identification of these three phases: $CoSb_3$ (white areas), AlSb (light grey areas) and AlCo (dark grey areas). Similarly, the BSE image from the sample C4 is displayed in **Fig.7** and also reveals three phases: CoSb (white areas), (Co) (light grey areas), AlCo (dark grey areas). It is interesting to note that these observations highlight the existing equilibria between these phases since each one is in contact with the two others. Thus, these observations confirm the presence of some three-phase equilibria in the Al-Co-Sb ternary diagram (**Table 3**). More specifically, this experimental study highlights the existence of a thermodynamic equilibrium between AlSb and $CoSb_3$, unpredicted by the calculation (**Fig.4**). This result is highly important for this work in which a coating is synthesized by the diffusion of aluminum at 600 °C inside the $CoSb_3$ substrate. Therefore, the thermodynamic equilibria at the alloy surface are the main factor influencing the process, the formation of phases [**13**]. According to this

new built ternary diagram, several phases can coexist in a thermodynamic equilibrium during the pack cementation process. This assumption has to be checked experimentally.

4.2. Coating synthesized by pack cementation

The cross-section SEM image of **Fig.8** and the corresponding X-ray elemental mapping present the coating obtained on the $CoSb_3$ substrate. This chemical characterization indicates that the synthesized coating is made of aluminum, cobalt and antimony. More accurately, the XRD characterization of **Fig.9** points out the two crystalline phases of the coating: AlSb is the major one and Al_9Co_2 is the minor one. These experimental observations confirm the predicted thermodynamic equilibrium between these two phases. The corresponding diffusion pathway of Al inside the $CoSb_3$ substrate during the pack cementation process can be plotted on the isothermal section of **Fig.10**. The equilibrium previously highlighted between AlSb and $CoSb_3$ justifies that AlSb is the major phase formed at 600 °C. Moreover, this phase can be in equilibrium with Al_9Co_2, the minor phase of this biphasic coating. Therefore, these results describe the possibility to produce a metallic coating from aluminum powder on the surface of the $CoSb_3$ thermoelectric material. The formation mechanisms of aluminide coatings are commonly described as follows [**25,26**]:

(i) Formation of aluminum chlorides by the reaction of the halide salt activator ($CrCl_3$) and the aluminum metal powder of the pack.

(ii) Transport of the aluminum chlorides towards the substrate by gas-phase diffusion.

(iii) Reaction leading to the deposition of aluminum at the substrate surface.

(iv) Diffusion of aluminum into the substrate with the formation of the aluminide coating.

(v) Diffusion of the reaction products from the substrate back to the pack.

In this work, the pack cementation process produces an aluminide surface layer made of AlSb and Al_9Co_2 on $CoSb_3$. This layer is synthesized with the objective to protect the substrate from oxidation in order to make thermoelectric generators usable under oxidative environments. Since the affinity of AlSb and Al_9Co_2 with oxygen has been already studied and established, this layer could be an appropriate protective layer able to keep oxygen, avoiding its diffusion throughout the substrate [**27-30**]. Indeed, Shibata *et al.* have shown that AlSb is extremely liable to be oxidized during an exposition in air at high temperature. They have described the mechanisms of the process in two steps that lead to the formation of an amorphous oxide [**31**]. Similarly, Wardé *et al.* have described the oxidation of Al_9Co_2 in a wide range of temperatures until 752 °C. They have observed the quick formation of Al-O bonds inducing the following steps: formation of an oxide film, dissolution of the film, oxygen desorption and dissolution into the Al_9Co_2 bulk [**32**]. Consequently, since the synthesized aluminide coating is made of these two crystalline phases, the lifespan extension of the thermoelectric material is expected in an oxidizing environment such as air atmosphere.

4.3. Oxidation of the aluminized $CoSb_3$ skutterudite

The aluminized $CoSb_3$ sample has been oxidized under a flow of synthetic air at 527 °C for 1000 h. The cross-section of the oxidized sample is presented in **Fig.11** with the corresponding X-ray elemental mapping. These characterizations reveal that the aluminized area at the top of the $CoSb_3$ substrate is fully oxidized since oxygen is identified on the whole thickness of the coating. The corresponding X-ray microanalysis obtained from EDS spots carried out inside the oxidized coating indicates an average oxygen atomic ratio of 43.8 at.%. More particularly, it is noticeable that there is no oxygen in the $CoSb_3$ substrate but only inside the coating whose affinity with oxygen is the highest one. This observation highlights

that the metallic coating acts as a barrier for oxygen and protects the $CoSb_3$ substrate from oxidation. The XRD patterns obtained after 1000 h of oxidation at 527 °C of the coated sample is presented in **Fig.12**. In comparison with the XRD patterns obtained before oxidation (**Fig.9**), we can note that AlSb, the main crystalline phase of the coating is still observable but the signal from the $CoSb_3$ substrate is sharply more pronounced although the thickness of the coating has not changed. This effect indicates that the penetration depth of the incident X-ray beam is higher through the surface layer that became less dense during the oxidation process. Indeed, it is well established that the penetration depth of an X-ray beam is linked to the density of the crossed material [**33, 34**]. Moreover, the XRD patterns of the oxidized sample also reveal the presence of some alumina (α-Al_2O_3) meaning that a part of the formed oxides has been crystallized. However, considering the amount of oxygen determined from X-ray microanalysis (43.8 %) and the X-ray elemental mapping obtained from EDS, it is obvious that the formed oxides are mainly amorphous and then unobservable by X-ray diffraction. This assumption is understandable considering the quite low oxidation temperature used in this study (527 °C). This temperature is appropriate to promote the diffusion of oxygen inside the metallic coating and the formation of some oxides but without any crystallization of the formed oxides that remain mainly amorphous. Due to their high affinity with oxygen, aluminum and antimony from AlSb, can be easily considered as the main elements involved in the oxides formation, e.g. producing Al_2O_3 and Sb_2O_3 / Sb_2O_4 [**29**]. However, the crystallization temperature for these oxides is higher than that used in this study, explaining why they can exist only in an amorphous state inside the surface layer [**35, 36**]. Nonetheless, the protection property of the synthesized coating is clearly evidenced and it makes the $CoSb_3$ skutterudite material usable under air environment at 527 °C for 1000 h. The aluminized surface layer acts as a protecting barrier for the substrate, avoiding the oxygen penetration. Consequently, the initial objective is reached, making this system interesting and powerful to

produce thermoelectric generators usable not only under vacuum for aerospace applications, but also on Earth in air environment.

5. Conclusion

This work has described the synthesis of an aluminide layer by pack cementation on $CoSb_3$ skutterudite. To reach this objective, the isothermal section at 600 °C of the Al-Co-Sb ternary diagram has been investigated for the first time to know the thermodynamic equilibria between the phases formed from these three elements. To confirm the predicted equilibria of the ternary system, several samples have been synthesized to explore the section. Particularly, the two-phases equilibrium between $CoSb_3$ and AlSb has been highlighted and some three-phases domains have been observed. From this work, the sequence of the phases formed during the pack cementation process has been highlighted and the experimental conditions of the process have been defined. The aluminide layer has been achieved on the $CoSb_3$ substrate. The structural investigations have shown that the coating is made of two crystalline phases, the major one is AlSb and the minor one is Al_9Co_2. Therefore, an appropriate corrosion behavior of the coated $CoSb_3$ has been observed under a flow of synthetic air at 527 °C for 1000 hours. The aluminide layer has act as a reservoir of aluminum for maintaining a protective Al_2O_3 scale on the material surface during the oxidation process. Consequently, the aluminized layer makes the $CoSb_3$ skutterudite an appropriate thermoelectric material for a use under an oxidative environment such as air.

6.Acknowledgments

The authors sincerely thank the French National Agency of Research (ANR) for the financial support of the Nanoskut project (ANR-12-PRGE-0008-01).

7. References

[**1**] M. Rull-Bravo, A. Moure, J.F. Fernandez, M. Martin-Gonzalez, Skutterudites as thermoelectric materials: revisited, RSC Adv. 52 (2015) 41653-41667.

[**2**] W. Liu, Q. Jie, H. Seok Kim, Z. Ren, Current progress and future challenges in thermoelectric power generation: From materials to devices, Acta Mater. 87 (2015) 357-376.

[**3**] J.W. Sharp, E.C. Jones, R.K. Williams, P.M. Martin, B.C. Sales, Thermoelectric properties of $CoSb_3$ and related alloys, J. Appl. Phys. 78 (1995) 1013-1018.

[**4**] T.M. Tritt, M.A. Subramanian, Thermoelectric Materials, Phenomena, and Applications: A Bird's Eye View, MRS Bull. 31(3) (2006) 188-194.

[**5**] J.X. Zhang, Q.M. Lu, K.G. Liu, L. Zhang, M.L. Zhou, Synthesis and thermoelectric properties of $CoSb_3$ compounds by spark plasma sintering, Mater. Lett. 58 (2004) 1981-1984.

[**6**] Y. Kawaharada, K. Kurosaki, M. Uno, S. Yamanaka, Thermoelectric properties of $CoSb_3$, J. Alloys Compd 315 (2001) 193-197.

[**7**] M. Zebarjadi, K. Esfarjani, M.S. Dresselhaus, Z.F. Ren, G. Chen, Perspectives on thermoelectrics: from fundamentals to device applications, Energy Environ. Sci. 5 (2012), 5147-5162.

[**8**] E. Godlewska, K. Zawadzka, A. Adamczyk, M. Mitoraj, K. Mars, Degradation of $CoSb_3$ in Air at Elevated Temperatures, Oxid Met 74 (2010) 113-124.

[**9**] R. Hara, S. Inoue, H.T. Kaibe, S. Sano, Aging effects of large-size n-type CoSb3 prepared by spark plasma sintering, J. Alloys Compd 349 (2003) 297-301.

[**10**] J. Leszczynski, K.T. Wojciechowski, A.L. Malecki, Studies on thermal decomposition and oxidation of $CoSb_3$, J Therm Anal Calorim 105 (2011) 211-222.

[**11**] D. Zhao, M. Zuo, Z. Wang, X. Teng, H. Geng, Protective properties of magnetron-sputtered Ti coating on $CoSb_3$ thermoelectric material, Appl. Surf. Sci. 305 (2014) 86-92.

[**12**] H. Dong, X. Li, X. Huang, Y. Zhou, W. Jiang, L. Chen, Improved oxidation resistance of thermoelectric skutterudites coated with composite glass, Ceram. Int. 39 (2013) 4551-4557.

[**13**] L. Portebois, S. Mathieu, Y. Bouizi, M. Vilasi, S. Mathieu, Effect of boron addition on the oxidation resistance of silicide protective coatings: A focus on boron location in as-coated and oxidised coated niobium alloys, Surf. Coat. Technol. 253 (2014) 292-299.

[**14**] B.M. Warnes, D.C. Punola, Clean diffusion coatings by chemical vapor deposition, Surf. Coat. Technol. 94–95 (1997) 1-6.

[**15**] Z. Xu, J. Dai, J. Niu, L. He, R. Mu, Z. Wang, Isothermal oxidation and hot corrosion behaviors of diffusion aluminide coatings deposited by chemical vapor deposition, J. Alloys Compd 637 (2015) 343-349.

[**16**] F. Stein, C. He, N. Dupin, Melting behaviour and homogeneity range of *B2* CoAl and updated thermodynamic description of the Al-Co system, Intermetallics 39 (2013) 58-68.

[**17**] R. Novakovic, T. Tanaka, Bulk and surface properties of Al–Co and Co–Ni liquid alloys, Physica B 371 (2006) 223-231.

[**18**] L.G. Zhang, H.M. Chen, H.Q. Dong, G.X. Huang, L.B. Liu, Z.P. Jin, Thermodynamic description of the Al–Sb–Y system, J. Alloys Compd 475 (2009) 233-237.

[**19**] T. Balakumar, M. Medraj, Thermodynamic modeling of the Mg–Al–Sb system, CALPHAD 29 (2005) 24-36.

[**20**] A.S. Bracker, M.J. Yang, B.R. Bennett, J.C. Culbertson, W.J. Moore, Surface reconstruction phase diagrams for InAs, AlSb, and GaSb, J. Cryst. Growth 220 (2000) 384-392.

[**21**] Y. Zhang, C. Li, Z. Du, T. Geng, The thermodynamic assessment of the Co-Sb system, CALPHAD 32 (2008) 56-63.

[**22**] M.E. Schlesinger, Thermodynamic Properties of Solid Binary Antimonides, Chem. Rev. 113 (2013) 8066-8092.

[**23**] P. Villars, K. Cenzual, Pearson's Crystal Data: Crystal Structure Database for Inorganic Compounds (on DVD), Release 2019/20, ASM International®, Materials Park, Ohio, USA.

[**24**] E. Alleno, E. Zehani, O. Rouleau, Metallurgical and thermoelectric properties in $Co_{1-x}Pd_xSb_3$ and $Co_{1-x}Ni_xSb_3$ revisited, J. Alloys Compd 572 (2013) 43-48.

[**25**] J.T. John, G.B. Kale, S.R. Bharadwaj, R.S. Srinivasa, P.K De, A kinetic model for iron aluminide coating by low pressure chemical vapor deposition: Part II. Model formulation, Thin Solid Films 466 (2004) 331-338.

[**26**] Y. Matsuoka, Y. Matsunaga, K. Nakagawa, Y. Tuda, S. Taniguchi, Growth Behavior of Coatings Formed by Vapor Phase Aluminizing Using Fe-Al Pellets of Varying Composition, Materials Transactions 47 (2006) 2341-2347.

[**27**] E.I. Vaughan, S. Addamane, D.M. Shima, G. Balakrishnan, A.A. Hecht, High-Resistivity Semi-insulating AlSb on GaAs Substrates Grown by Molecular Beam Epitaxy, J. Electron. Mater. 45 (2016) 2025-2030.

[**28**] J. Nilsson, A.R. Landa-Canovas, S. Hansen, A. Andersson, An Investigation of the Al–Sb–V–W–Oxide System for Propane Ammoxidation, J. Catal. 186 (1999) 442-457.

[**29**] J. Nakata, T. Shibata, Y. Nanishi, M. Fujimoto, Suppression of AlSb oxidation with hydrocarbon passivation layer induced by MeV-He^+ irradiation, J. Appl. Phys. 76 (1994) 2078-2085.

[**30**] S. Alarcón Villaseca, L.N. Serkovic Loli, J. Ledieu, V. Fournée, P. Gille, J.M. Dubois, E. Gaudry, Oxygen adsorption on the Al_9Co_2(001) surface: first-principles and STM study, J. Phys.: Condens. Matter. 25 (2013) 355003.

[**31**] T. Shibata, J. Nakata, Y. Nanishi, M. Fujimoto, A Rutherford Backscattering Spectroscopic Study of the Aluminum Antimonide Oxidation Process in Air, Jpn. J. Appl. Phys. 33 (1994) 1767-1772.

[**32**] M. Wardé, M. Herinx, J. Ledieu, L.N. Serkovic Loli, V. Fournée, P. Gille, S. Le Moal, M.-G. Barthés-Labrousse, Adsorption of O_2 and C_2H_n (n = 2, 4, 6) on the Al_9Co_2(0 0 1) and o-$Al_{13}Co_4$(1 0 0) complex metallic alloy surfaces, Appl. Surf. Sci. 357 (2015) 1666-1675.

[**33**] L.G. Parratt, Surface Studies of Solids by Total Reflection of X-Rays, Phys. Rev. 95 (1954) 359-369.

[**34**] Z.H. Kalman, L.A. Johnson, J.B. Wachtman, Density determination of thin coatings by X-ray methods, J. Amer. Ceram. Soc. 72 (1989) 1170-1174.

[**35**] S. Jakschik, U. Schroeder, T. Hecht, M. Gutsche, H. Seidl, J.W. Bartha, Crystallization behavior of thin ALD-Al_2O_3 films, Thin Solid Films 425 (2003) 216-220.

[**36**] R.G. Orman, D. Holland, Thermal phase transitions in antimony (III) oxides, J. Solid State Chem. 180 (2007) 2587-2596.

Figure captions

Fig.1. Co-Sb equilibrium phase diagram [21].

Fig.2. Al-Co equilibrium phase diagram [16].

Fig.3. Al-Sb equilibrium phase diagram [19].

Fig.4. Isothermal section at 600 °C of the Al-Co-Sb ternary equilibrium diagram. Position of the chemical compositions experimentally studied.

Fig.5. XRD patterns of the eight chemical compositions identified on the isothermal section of Fig.4.

Fig.6. Back-scattered electron (BSE) image and EDS characterization of the C1 sample after thermal treatment at 600 °C.

Fig.7. Back-scattered electron (BSE) image and EDS characterization of the C4 sample after thermal treatment at 600 °C.

Fig.8. Cross-section SEM image, EDS characterization and X-ray elemental mapping of the aluminizing layer synthesized on the $CoSb_3$ substrate.

Fig.9. XRD patterns of the aluminizing layer synthesized on the $CoSb_3$ substrate.

Fig.10. Isothermal section at 600 °C of the Al-Co-Sb ternary equilibrium diagram. Diffusion way of Al inside $CoSb_3$ during the pack cementation process.

Fig.11. Cross-section SEM image, EDS characterization and X-ray elemental mapping of the aluminized $CoSb_3$ sample after oxidation at 527 °C for 1000 hours.

Fig.12. XRD patterns of the aluminized $CoSb_3$ surface after oxidation at 527 °C for 1000 hours.

Fig.1

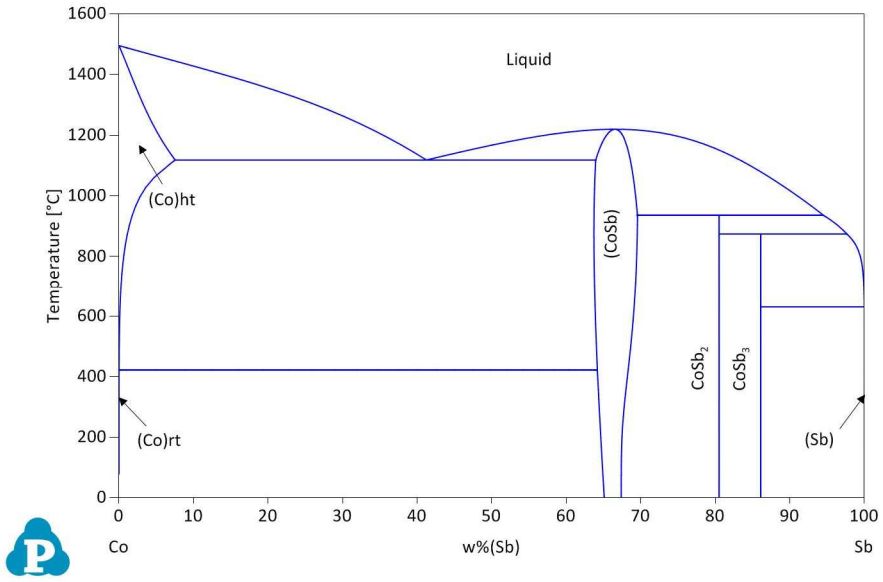
Liquid
(Co)ht
(Co)rt
(CoSb)
CoSb2
CoSb3
(Sb)
Temperature [°C]
1600
1400
1200
1000
800
600
400
200
0
0
10
20
30
40
50
60
70
80
90
100
Co
w%(Sb)
Sb

Fig.2

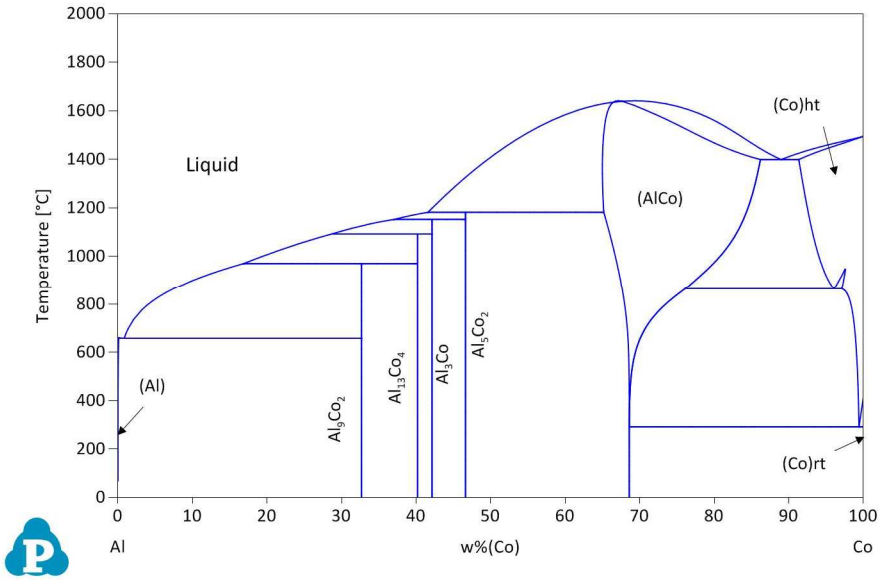
Temperature [°C]
2000
1800
1600
1400
1200
1000
800
600
400
200
0
Liquid
(Co)ht
(AlCo)
(Al)
Al_9Co_2
$Al_{13}Co_4$
Al_3Co
Al_5Co_2
(Co)rt
0
10
20
30
40
50
60
70
80
90
100
Al
w%(Co)
Co

Fig.3

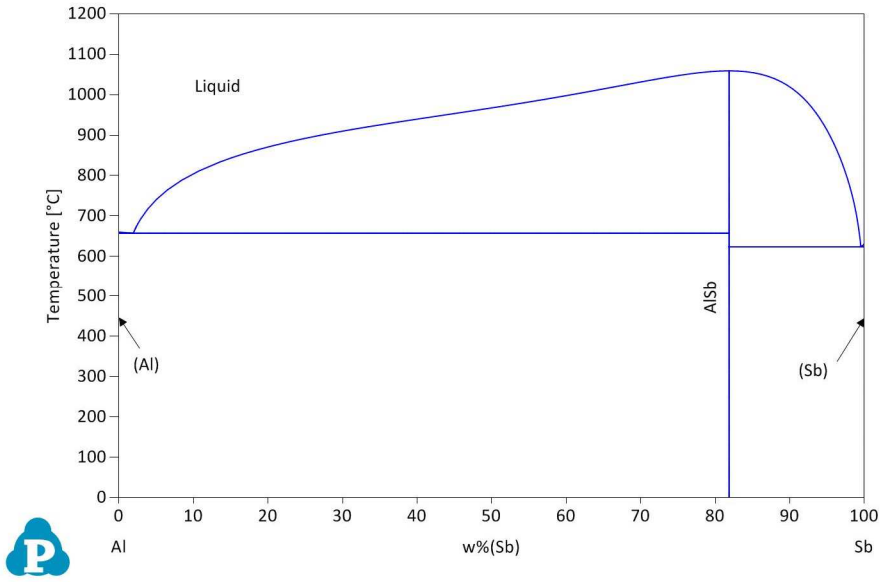
Liquid
Temperature [°C]
1200
1100
1000
900
800
700
600
500
400
300
200
100
0
(Al)
AlSb
(Sb)
0
10
20
30
40
50
60
70
80
90
100
Al
w%(Sb)
Sb

Fig.4

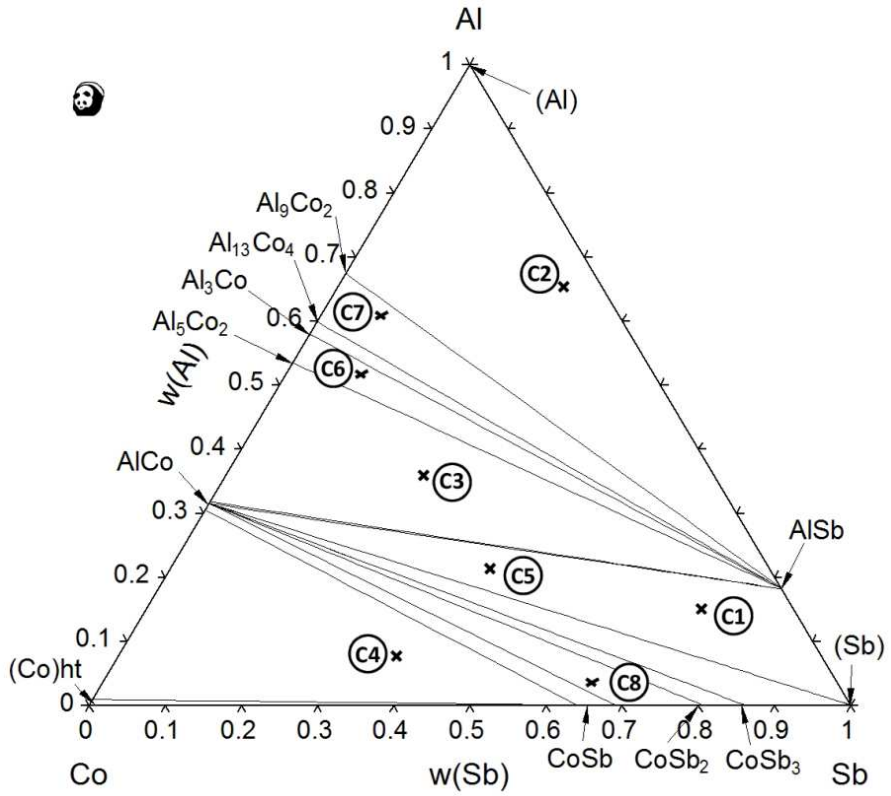
Al
1
(Al)
0.9
0.8
Al_9Co_2
$Al_{13}Co_4$
0.7
Al_3Co
0.6
Al_5Co_2
w(Al)
0.5
0.4
AlCo
0.3
0.2
0.1
(Co)ht
0
C1
C2
C3
C4
C5
C6
C7
C8
AlSb
(Sb)
0
0.1
0.2
0.3
0.4
0.5
0.6
0.7
0.8
0.9
1
CoSb
$CoSb_2$
$CoSb_3$
Co
w(Sb)
Sb

Fig.5

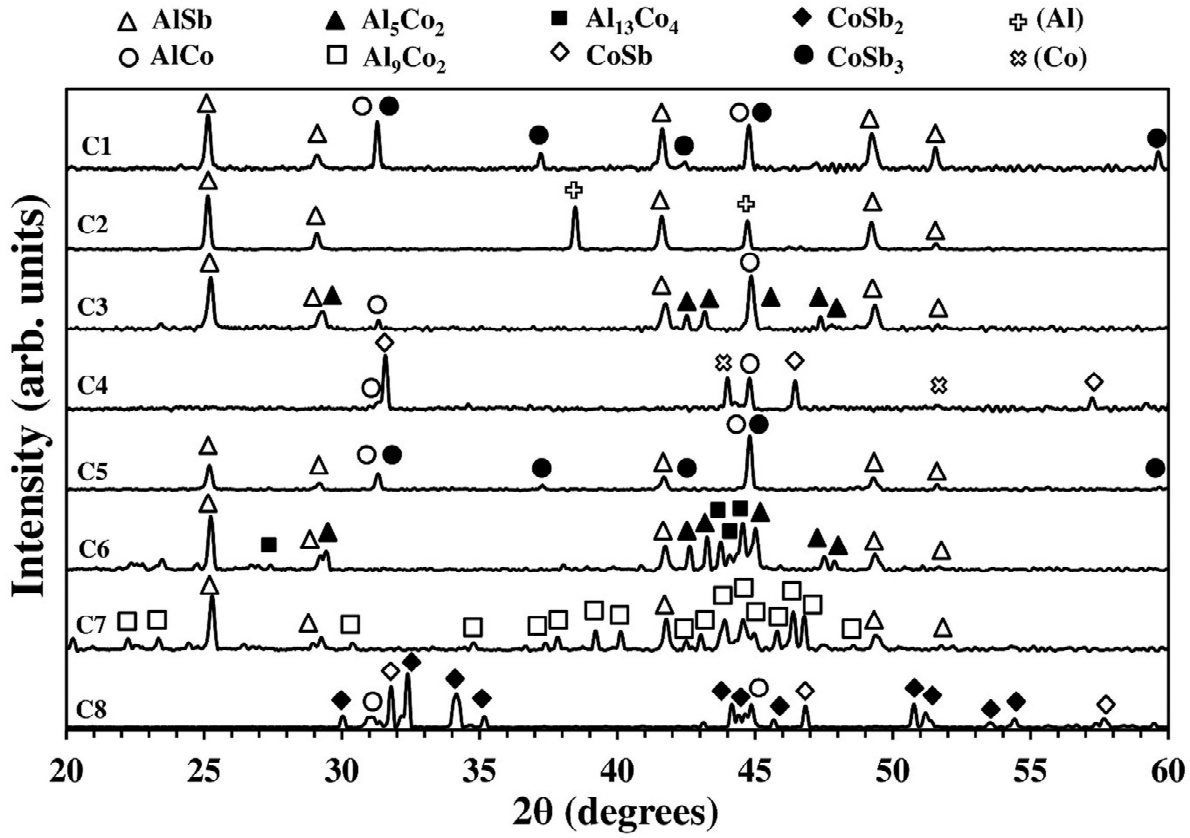
△ AlSb
○ AlCo
▲ Al_5Co_2
□ Al_9Co_2
■ $Al_{13}Co_4$
◇ CoSb
◆ $CoSb_2$
● $CoSb_3$
✠ (Al)
⊠ (Co)
C1
C2
C3
C4
C5
C6
C7
C8
Intensity (arb. units)
20
25
30
35
40
45
50
55
60
2θ (degrees)

Fig.6

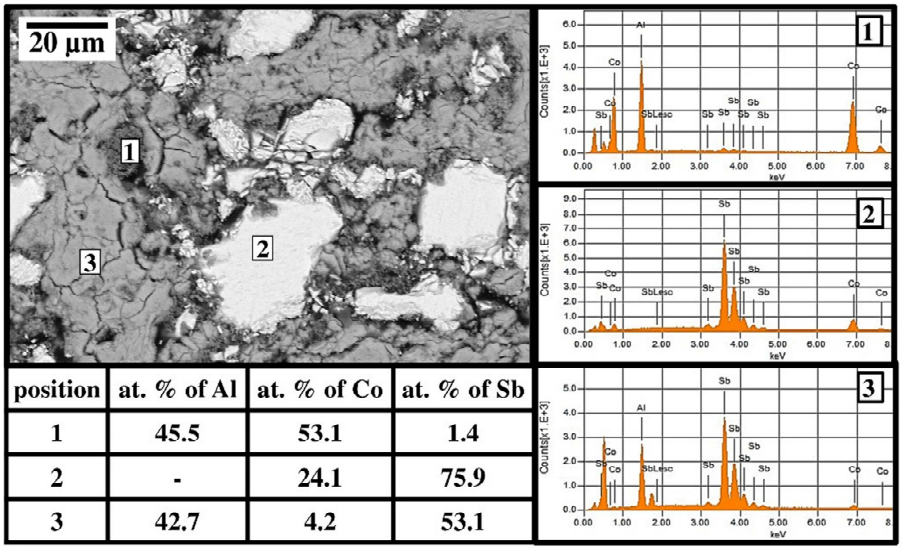

position	at. % of Al	at. % of Co	at. % of Sb
1	45.5	53.1	1.4
2	-	24.1	75.9
3	42.7	4.2	53.1

Fig.7

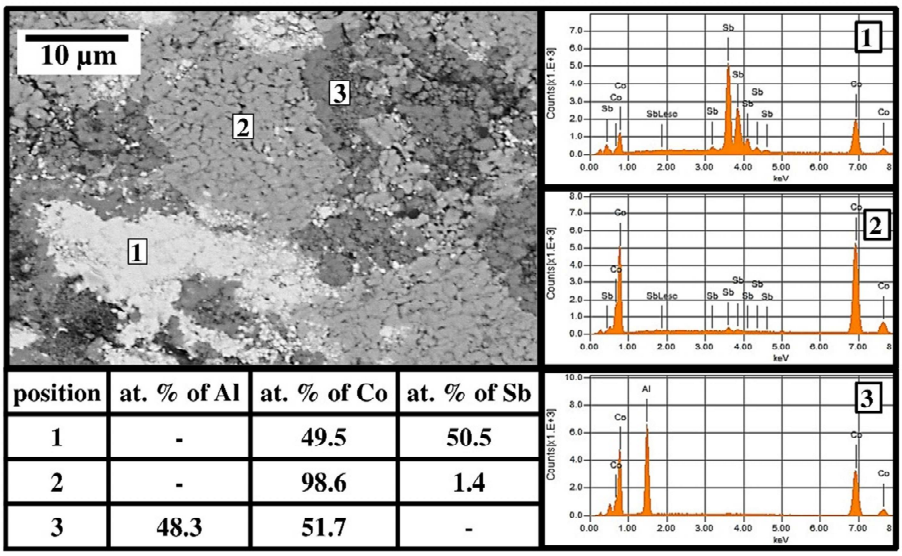

position	at. % of Al	at. % of Co	at. % of Sb
1	-	49.5	50.5
2	-	98.6	1.4
3	48.3	51.7	-

Fig.8

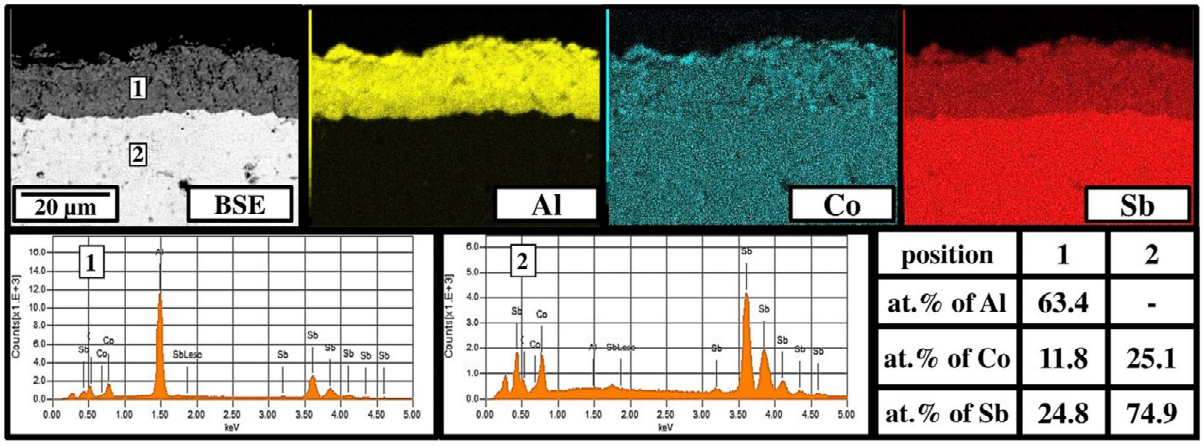

position	1	2
at.% of Al	63.4	-
at.% of Co	11.8	25.1
at.% of Sb	24.8	74.9

Fig.9

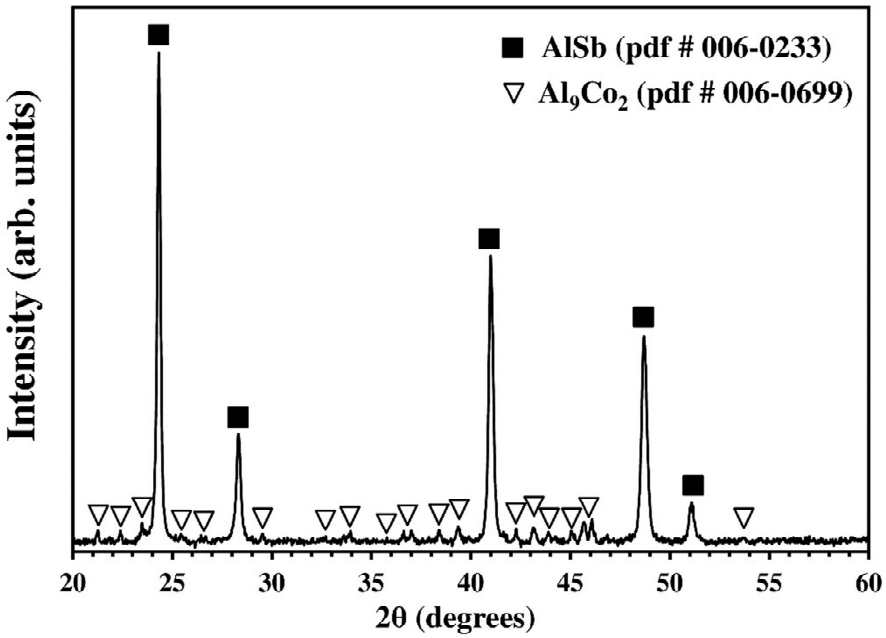
AlSb (pdf # 006-0233)
Al9Co2 (pdf # 006-0699)
Intensity (arb. units)
20
25
30
35
40
45
50
55
60
2θ (degrees)

Fig.10

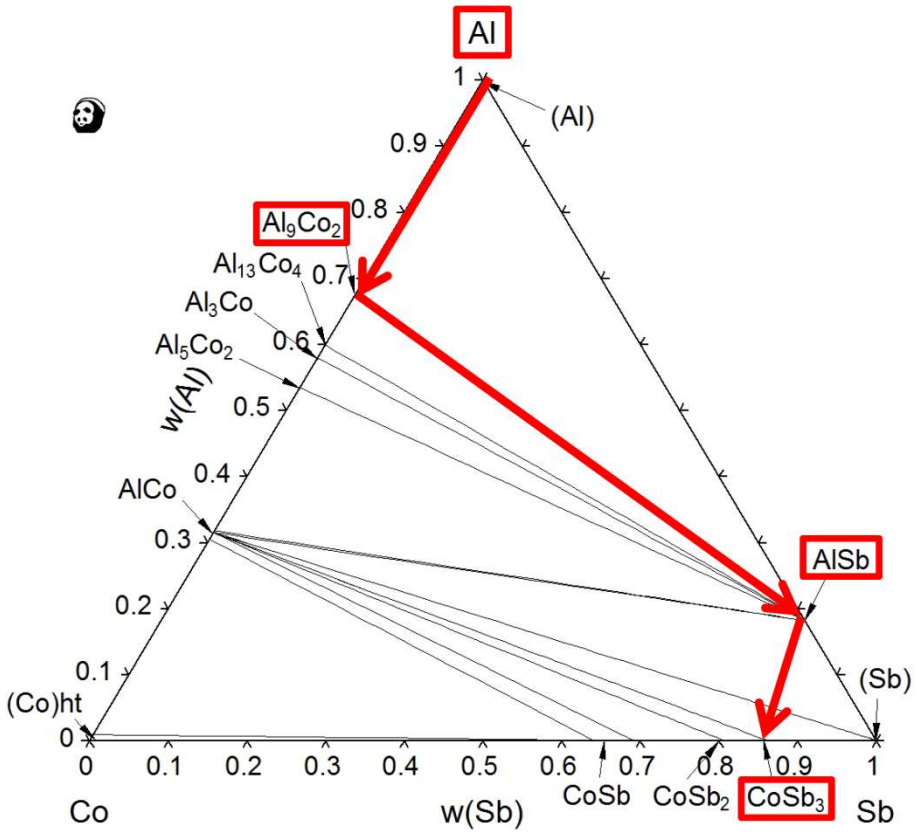
Al
(Al)
Al9Co2
Al13Co4
Al3Co
Al5Co2
AlCo
(Co)ht
w(Al)
AlSb
(Sb)
Co
w(Sb)
Sb
CoSb
CoSb2
CoSb3
0
0.1
0.2
0.3
0.4
0.5
0.6
0.7
0.8
0.9
1

Fig.11

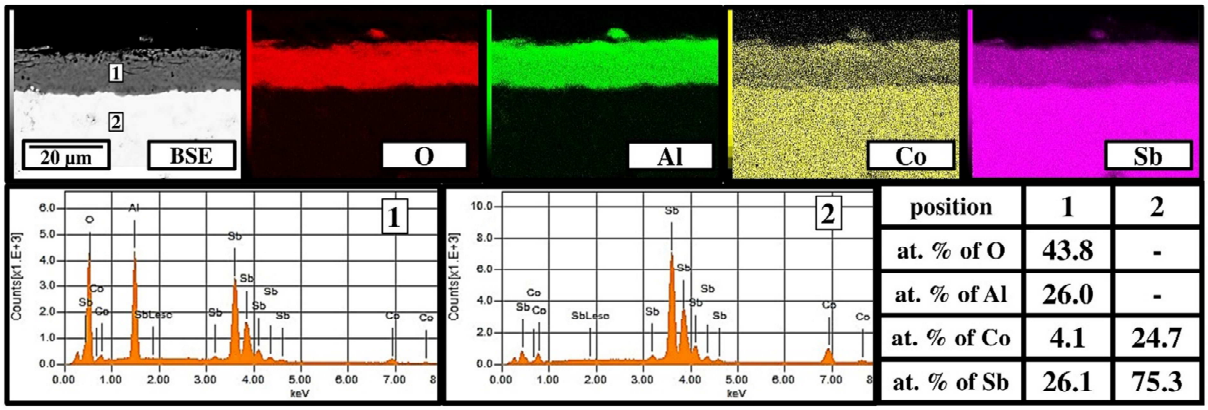

position	1	2
at. % of O	43.8	-
at. % of Al	26.0	-
at. % of Co	4.1	24.7
at. % of Sb	26.1	75.3

Fi.g.12

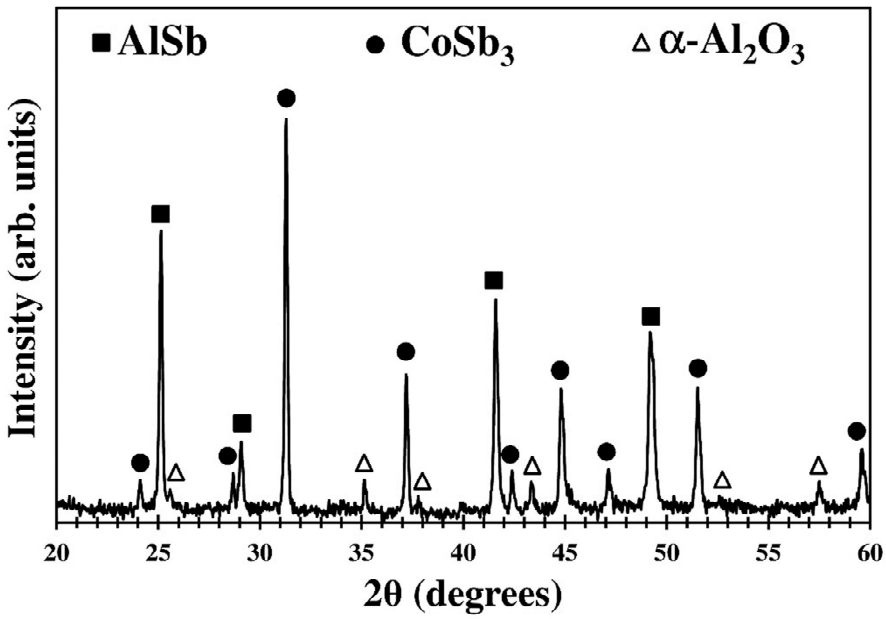
AlSb
CoSb3
α-Al2O3
Intensity (arb. units)
20
25
30
35
40
45
50
55
60
2θ (degrees)

Table captions

Table 1. Phases of the Co-Sb, Al-Co and Al-Sb systems [**23**]

Table 2. Equilibria between phases of the Co-Sb, Al-Co and Al-Sb systems [**16,19,21**]

Table 3. Chemical compositions of the pellets used in the experimental thermodynamic study and the phases observed after the thermal treatment at 600 °C

w

Table 1.

Phase	Formula	Prototype	Pearson symbol	Space group
(Co) ht (αCo)	Co	Cu	cF4	Fm-3m
(Co) rt (εCo)	Co	Mg	hP2	$P6_3/mmc$
β CoSb	CoSb	NiAs	hP4	$P6_3/mmc$
γ $CoSb_2$ ht	$CoSb_2$	$FeAs_2$	oP6	Pnnm
γ' $CoSb_2$ rt	$CoSb_2$	$CoSb_2$	mP12	$P12_1/c1$
δ $CoSb_3$	$CoSb_3$	$CoAs_3$	cI32	Im-3
(Sb)	Sb	As	hR6	R-3m
(Al)	Al	Cu	cF4	Fm-3m
Co_2Al_9	Co_2Al_9	Co_2Al_9	mP22	$P12_1/c1$
Co_4Al_{13} rt	Co_4Al_{13}	Co_4Al_{13}	oP102	$Pmn2_1$
Co_2Al_5	Co_2Al_5	Co_2Al_5	hP28	$P6_3/mmc$
β CoAl	CoAl	CsCl	cP2	Pm-3m
AlSb	AlSb	ZnS	cF8	F-43m

Table 2.

Invariant equilibria	% at. Sb, respectively			Temperature (°C)	Reaction
L ↔ (Co) ht				1495	Melting
(Co) ht ↔ (Co) rt				422	Allotropic
L = (Co) ht + CoSb	25.4	3.8	46.2	1118	Eutectic
L ↔ CoSb	49.1	49.1		1220	Congruent
L + CoSb = $CoSb_2$ ht	89.3	52.5	66.7	936	Peritectic
L + $CoSb_2$ ht = $CoSb_3$	85.3	66.7	75	874	Peritectic
L = $CoSb_3$ + (Sb)	99.98	75	100	630.7	Eutectic
L ↔ (Sb)		100		630.755	Melting
Invariant equilibria	**% at. Co, respectively**			**Temperature (°C)**	**Reaction**
L ↔ (Al)				660.452	Melting
L = (Al) + Co_2Al_9	0.4	0.04	18.2	658	Eutectic
(Co) ht = CoAl + (Co) ht	91.8	59.3	93.9	865	Eutectoid
L + Co_4Al_{13} = Co_2Al_9	8.5	23.5	18.2	970	Peritectic
L + $CoAl_3$ = Co_4Al_{13}	15.6	25	23.5	1093	Peritectic
L + Co_2Al_5 = $CoAl_3$	21.2	28.6	25	1153	Peritectic
L + CoAl = Co_2Al_5	24.6	46.2	28.6	1180	Peritectic
L = CoAl		48.3		1671	Congruent
L = CoAl + (Co) ht	78.7	74.1	82.8	1399	Eutectic
(Co) ht = CoAl + (Co) rt	98.7	50	100	300	Eutectoid
Invariant equilibria	**% at. Sb, respectively**			**Temperature (°C)**	**Reaction**
L = (Al) +AlSb	0.34		50	658.3	Eutectic
L = AlSb		50		1055.4	Congruent
L = AlSb + (Sb)	97.4	50	100	620	Eutectic

Table 3.

Sample	Weight contents in			Phases in equilibrium after the thermal treatment at 600°C
	Al	Co	Sb	
C1	15%	12%	73%	AlSb + AlCo + $CoSb_3$
C2	65%	5%	30%	AlSb + (Al)
C3	35%	39%	26%	AlSb + Al_5Co_2 + AlCo
C4	8%	55%	37%	AlCo + CoSb + (Co)
C5	21%	36%	43%	AlSb + AlCo + $CoSb_3$
C6	52%	38%	10%	AlSb + Al_5Co_2 + $Al_{13}Co_4$
C7	60%	32%	8%	AlSb + Al_9Co_2
C8	4%	32%	64%	CoSb + $CoSb_2$ + AlCo